Am J Cancer Res 2023;13(6):2213-2233
www.ajcr.us /ISSN:2156-6976/ajcr0149989

Original Article

Exploring the correlation of glycolysis-related chondroitin polymerizing factor (*CHPF*) with clinical characteristics, immune infiltration, and cuproptosis in bladder cancer

Quliang Zhong[1,2], Kehua Jiang[3], Facai Zhang[4], Yuan Tian[2], Jiang Gu[2], Tao Li[2], Xulong Chen[2], Jianjun Yang[2], Fa Sun[1,3]

[1]Guizhou Medical University, Guiyang 550001, Guizhou, China; [2]Department of Urology, Affiliated Hospital of Guizhou Medical University, Guiyang 550001, Guizhou, China; [3]Guizhou Provincial People's Hospital, Guiyang 550002, Guizhou, China; [4]Department of Urology, Zhejiang Provincial People's Hospital, Hangzhou 310014, Zhejiang, China

Received March 5, 2023; Accepted May 13, 2023; Epub June 15, 2023; Published June 30, 2023

Abstract: Bladder cancer (BLCA) is a common malignant neoplasm of the urinary system. Glycolysis is an essential metabolic pathway regulated by various genes with implications for tumor progression and immune escape. Scoring the glycolysis for each sample in the TCGA-BLCA dataset was done using the ssGSEA algorithm for quantification. The results showed that the score in BLCA tissues was markedly greater than those in adjacent tissues. Additionally, the score was found to be correlated with metastasis and high pathological stage. Functional enrichment analyses of the glycolysis-related genes showed they were related to roles associated with tumor metastasis, glucose metabolism, cuproptosis, and tumor immunotherapy in BLCA. Using 3 different machine learning algorithms, we identified chondroitin polymerizing factor (*CHPF*) as a central glycolytic gene with high expression in BLCA. In addition, we showed *CHPF* is a valuable diagnostic marker of BLCA with an area under the ROC (AUC) of 0.81. Sequencing BLCA 5637 cells after siRNA-mediated *CHPF* silencing and bioinformatics revealed that *CHPF* positively correlated with the markers of epithelial-to-mesenchymal transformation (EMT), glycometabolism-related enzymes, and immune cell infiltration. In addition, *CHPF* silencing inhibited the infiltration of multiple immune cells in BLCA. Genes that promote cuproptosis negatively correlated with *CHPF* expression and were up-regulated after *CHPF* silencing. High *CHPF* expression was a risk factor for overall and progression-free survival of patients who received immunotherapy for BLCA. Finally, using immunohistochemistry, we demonstrated that the CHPF protein had high expression in BLCA, increasing in high-grade tumors and those with muscle invasion. The CHPF expression levels were also positively associated with ^{18}F-fluorodeoxyglucose uptake in PET/CT images. We conclude that the glycolysis-related gene *CHPF* is an effective diagnostic and treatment target for BLCA.

Keywords: Bladder cancer, glycolysis, immunotherapy, immune microenvironment, cuproptosis

Introduction

Bladder cancer (BLCA) is the 10th most common malignant neoplasm worldwide. The GLOBOCAN 2018 suggests BLCA has an increasing incidence and mortality rate with each passing year, accounting for 3.0% of all newly diagnosed malignant tumors and 2.1% of all tumor-related deaths [1, 2]. Most patients with BLCA initially present with its non-muscle invasive variant and typically undergo transurethral resection and chemotherapy to improve prognosis. A few patients, by contrast, have the muscle-invasive subtype of BLCA at initial diagnosis and undergo radical cystectomy and chemoradiotherapy. Although more than 50% of patients with either subtype experience postoperative recurrence within 5 years [3, 4], those with the muscle-invasive subtype also develop metastases, a common feature of BLCA progression. Thus, patients with the muscle-invasive variant and distant metastases have a 5-year survival rate of only about 5%, despite radical surgical treatment [5, 6]. Early detection of BLCA metastases remains challenging for numerous reasons, such as low accuracy and

high invasiveness of available methods. Hence, only 4% of newly diagnosed patients with BLCA per year are identified as having metastases [2], underscoring the need for effective diagnostic tools. The field of cancer immunotherapy is experiencing remarkable success owing to the utilization of immune checkpoint inhibitor (ICI) therapy as cancer treatment [7, 8]. Since the evidence indicates the response rate of this therapy is related to the tumor microenvironment and the composition of immune cells that infiltrate it, identifying the diagnostic and immune-related markers of BLCA should facilitate early diagnosis of the disease and making timely therapy plans for patients.

Glucose is the essential energy-supplying substance in the human body and can supply energy via glycolysis, pentose phosphate, and oxidative phosphorylation pathways. While normal human cells obtain energy preferably by converting glucose into pyruvate under aerobic conditions, cancer cells tend to generate it by converting glucose into lactate, regardless of oxygen presence, which is called the Warburg effect [9]. Accumulating evidence suggests that glycolysis promotes the occurrence and progression of tumors and tumor immune escape [10, 11]. Among the genes associated with the glycolysis metabolism of tumor cells is the chondroitin polymerizing factor (CHPF) gene. It contains four discrete exons in the 2q35-q36 region of human chromosomes and encodes a glycosyltransferase that catalyzes the elongation of chondroitin sulfate [12]. Because this gene is misregulated in many cancer cells, it affects their proliferation, apoptosis, and migration, contributing to tumor development and evolution [13-15]. Hence, targeting the glycolysis-related genes such as CHPF combined with tumor immunotherapy could become an effective method for cancer treatment.

Copper is an essential trace element involved in many biological processes. Excess copper in cells binds to the acylated components of the tricarboxylic acid (TCA) cycle, provoking proteotoxic stress and ultimately causing cell death called cuproptosis [16, 17]. Interestingly, high copper levels are also associated with the occurrence and progression of bladder cancer [18].

However, the function and mechanism of *CHPF* in BLCA remains unclear. The single-sample gene set enrichment analysis (ssGSEA) algorithm was used to assess the differences in glycolysis feature scores between BLCA tissues and adjacent tissues using publicly available RNA-Seq datasets. In addition, 200 glycolysis genes were comprehensively analyzed by multiple machine learning methods. These experiments showed that among the analyzed genes, *CHPF* had the most significant diagnostic value for BLCA. The differences in *CHPF* expression between different clinical groups of patients with BLCA and the influence on patient survival were also explored. Gene Ontology (GO), Kyoto Encyclopedia of Genes and Genomes (KEGG), and GSEA enrichment analyses unveiled that glycolysis genes in BLCA were related to glycometabolism, cuproptosis, and tumor immunotherapy. The potential roles of *CHPF* were explored in each of the 3 identified biological processes. Finally, *CHPF* expression in BLCA and its correlation with clinical characteristics and ^{18}F-fluorodeoxyglucose (^{18}F-FDG) uptake were verified by immunohistochemistry (IHC) staining.

Materials and methods

Data collection and processing

Figure 1 depicts the main experimental steps performed in this study. The Cancer Genome Atlas (TCGA) database (https://portal.gdc.Cancer.gov) was mined for RNA-seq expression, clinical, and survival data. The data were normalized and subjected to $\log_2$ conversion. The glycolysis marker gene set (HALLMARK_GLYCOLYSIS) [Liberzon A] was obtained from the Molecular Signatures Database (MSigDB). Two immunotherapy datasets containing complete clinical data were retrieved from public sources to assess the association between *CHPF* expression and immunotherapy responses: the IMvigor 210 dataset, advanced urothelial carcinoma treated with atezolizumab (previously published studies), and the GSE176307 dataset, metastatic urothelial carcinoma treated with immune checkpoint blockade (Gene Expression Omnibus database).

Identification of candidate markers

Briefly, the glycolysis marker score for each BLCA sample was quantified using the ssGSEA algorithm, and the score differences between BLCA and adjacent tissues were assessed. The

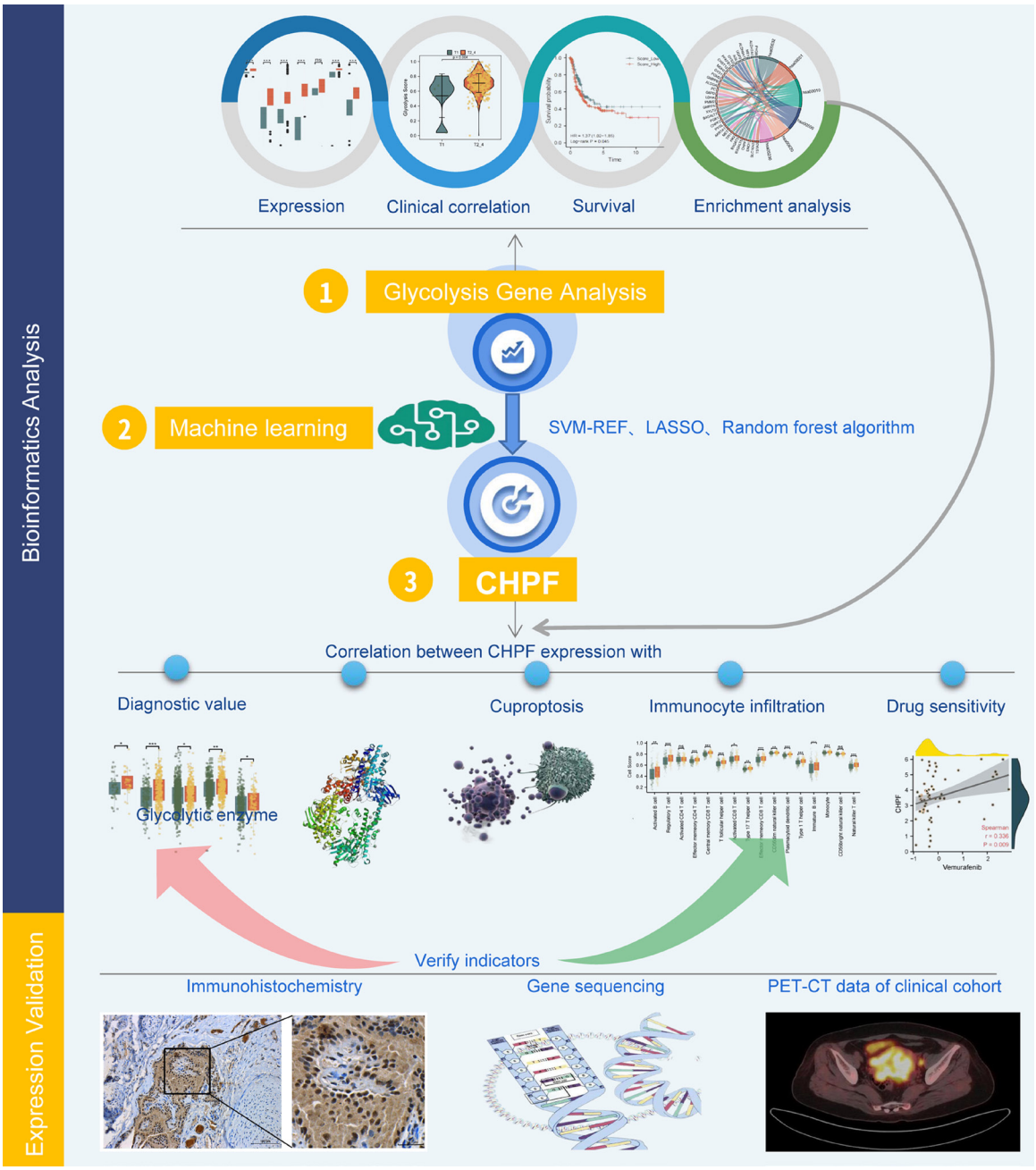

Figure 1. The workflow of this study.

correlation of the glycolysis marker score in BLCA with the clinical and pathological stages of the disease was also investigated. Next, the expression differences between BLCA and paired adjacent paracancerous tissues were explored for each gene. A total of 50 genes were identified based on the inclusion criterion of $|\log_2 FC| < 1$ and $P < 0.05$. These genes were analyzed by 3 machine learning algorithms: support vector machine recursive feature elimination (SVM-RFE), least absolute shrinkage and selection operator (LASSO) regression, and random forest machine learning algorithms, and the intersection was taken for the subsequent analysis.

Correlation between CHPF expression and clinical characteristics in BLCA

The R package limma was used to compare *CHPF* expression between malignant and noncancerous tissues in 33 types of cancer and

between paired cancerous and paracancerous tissues. The correlation between *CHPF* expression and clinical characteristics, such as clinical and pathological stages, was estimated. Finally, the receiver operating characteristic (ROC) curve representing the diagnostic value of *CHPF* in different tumors was calculated and visualized with the pROC package version 1.17.0.1.

Survival analysis

Univariate Cox regression analysis was performed using the R package survival to determine the correlation of the abovementioned indexes with the overall survival (OS) (time from the initiation of treatment to death due to any cause) and progression-free survival (PFS) (time from the initiation of treatment to disease progression or death due to any cause) of patients with BLCA. These data estimated the clinical value of glycolysis characteristic scores and *CHPF* expression in predicting patient survival. The hazard ratio (HR) > 1 indicated that an index was a factor that could induce patient death.

Functional enrichment analysis

Glycolysis markers obtained from the MSigDB database were subject to GSEA, GO, and KEGG enrichment analyses with the clusterProfiler package. The GO analysis inferred biological process (BP), cellular component (CC), and molecular function (MF) for each gene. The data were visualized by the ggplot2 package.

Correlation analysis

The matrix score, immune score, and tumor purity were estimated for each sample across multiple BLCA datasets using the ESTIMATE software package in RStudio. A total of 19 glycolysis-related transporters and other enzymes and 16 cuproptosis-related genes were collected from published sources. Their correlation with *CHPF* expression in BLCA was calculated by the Pearson correlation coefficient and the *t* test.

Immune infiltration analysis

The gene set variation analysis (GSVA) package was utilized for ssGSEA to estimate the infiltration abundance of 27 immune cells in BLCA tissues. The relationship between *CHPF* expression and the quantified immune-infiltrating cells was assessed with the Pearson correlation coefficient. Finally, the differences in the infiltration abundance of immune cells between the high- and low-*CHPF* expression groups in BLCA were also examined.

Determination of predicted sensitivity to therapeutic drugs

The Genomics of Drug Sensitivity in Cancer (GDSC) database (https://www.cancerrxgene.org/) encompasses drug sensitivity data for some 75,000 experiments, with sensitivity data of 138 anticancer drugs across 700 cancer cell lines. Sensitivity to various drugs was predicted with the R package pRRophetic by calculating the half-maximal inhibitory concentration (IC50) using a ridge regression model according to gene expression data.

Immunotherapy response analysis

Two independent immunotherapy datasets (GSE176307 and IMvigor 210), containing sequencing data, clinical survival information, and treatment response of patients with urothelial carcinoma, were used for the analysis. The treatment response cohort was involved in the data related to complete response (CR) and partial response (PR), while the non-response cohort was involved in the data related to stable disease (SD) and progressive disease (PD). The differences in *CHPF* expression between the treatment response and non-response cohorts were evaluated by the *t* test. Finally, the influence of *CHPF* expression on the survival of patients in the treatment cohort was assessed with the R package survival.

Collection of clinical samples

For this retrospective study, clinical data (e.g., age and TNM stage) of 33 patients with BLCA treated at Guizhou Medical University, Guiyang, China, from January 2022 to November 2022 were retrieved and evaluated. ^{18}F-FDG positron emission tomography/computed tomography (^{18}F-FDG-PET/CT) images of 17 patients were also analyzed based on the IHC scores of the corresponding resected tissues to explore the potential influence of *CHPF* expression on glycolysis. This study was approved by the

Research Ethics Committee of Guizhou Medical University (No. 2022-305).

Cell transfection, RNA extraction, and reverse transcription-quantitative polymerase chain reaction

Transfection experiments were performed using small interfering RNAs (siRNAs) against *CHPF* and negative control siRNAs (designed and synthesized by Huzhou Hippo Biotechnology Co., Ltd., China). Transfection was carried out using RNAiMAX (Invitrogen, Carlsbad, CA, USA). Total RNA was isolated using the TRIzol reagent (Ambion, Foster City, CA, USA) and reverse transcribed into cDNA using the ReverTra Ace qPCR RT Master Mix with a gDNA Remover (Toyobo, Co., Ltd., Osaka, Japan). Quantitative PCR (qPCR) was done with 2× SYBR Green qPCR Master Mix (Low ROX) (Wuhan Servicebio Technology Co., Ltd., Wuhan, China) in a 7500 Fast Dx Real-Time PCR Instrument (Applied Biosystems, Foster City, CA, USA). The primers used for PCR amplification were as follows: *CHPF*, forward 5'-GGAACGCACGTACCAGGAG-3' and reverse 5'-CGGGATGGTGCTGGAATACC-3'; *GADPH*, forward 5'-CATGTACGTTGCTATCCAGGC-3' and reverse 5'-CTCCTTAATGTCACGCACGAT-3'; and siCHPF sequence: UUCUCCGAACGUGUCACGUdTdT. The internal control for normalization was the *GADPH* gene, and the $2^{-\Delta\Delta Cq}$ method was applied to calculate relative gene expression levels.

Sequencing human bladder cancer cell line 5637 after CHPF silencing

The efficiency of *CHPF* knockdown was verified with a qPCR assay, and 3 pairs of transfected human bladder cancer 5637 cells were sent to Shanghai Biotechnology Corporation, China, for whole-genome sequencing. The resulting data were analyzed to investigate changes in gene expression in the human bladder cancer cell line 5637 after *CHPF* silencing.

Statistical analysis

GraphPad Prism 8.0 software (GraphPad Software Inc.) was used for statistical analysis. All data were expressed as mean ± standard deviation (SD). Differences between two groups were analyzed using a paired and 2-tailed unpaired *t* test, and those between three or more groups were with one-way analysis of variance (ANOVA). The correlation analysis was performed by Spearman rank correlation. Statistical significance was inferred when $P < 0.05$.

Results

The correlation between glycolysis feature scores and clinicopathological features in BLCA tissues

We quantified the feature scores of each sample from the TCGA-BLCA dataset using ssGSEA and investigated the differences in glycolysis feature scores between tumor and adjacent tissues (**Figure 2A**). We also explored the differences in glycolysis feature scores among various clinical feature groups of BLCA. These differences allowed us to assess the significance of glycolysis features in the disease. The scores of BLCA tissues in T3 and T4 category were significantly higher than those in the T1 and T2 (**Figure 2B**, $P = 0.032$). The scores of BLCA tissues with lymph node metastases were higher than those without metastasis (**Figure 2C**, $P = 0.093$) and rose further for those with distant metastasis (**Figure 2D**, $P = 0.03$). Furthermore, the scores of stage III and IV BLCA tissues were significantly higher than those of stage I and II (**Figure 2E**, $P < 0.001$). Similarly, the scores of tissues with tumor invasion into the muscularis propria were significantly higher than those without (**Figure 2F**, $P < 0.001$). Survival analysis was done to determine the influence of glycolysis characteristic scores on the survival of patients with BLCA, revealing a high score is a risk factor for the OS and PFS of the patients (**Figure 2G**, **2H**). These results show glycolysis feature score relates to tumor invasion and higher pathological stages, revealing the importance of glycolysis for BLCA development.

Enrichment analysis of glycolysis gene sets

Glycolysis-related genes from the TCGA-BLCA cohort were investigated with GO and KEGG enrichment analyses to evaluate their biological roles. These genes were mainly involved in glycolysis and glycometabolism and functions associated with cell death in response to oxidative stress, response to copper ion, and copper ion binding. They also predominantly participated in glycolysis/gluconeogenesis, pyruvate and

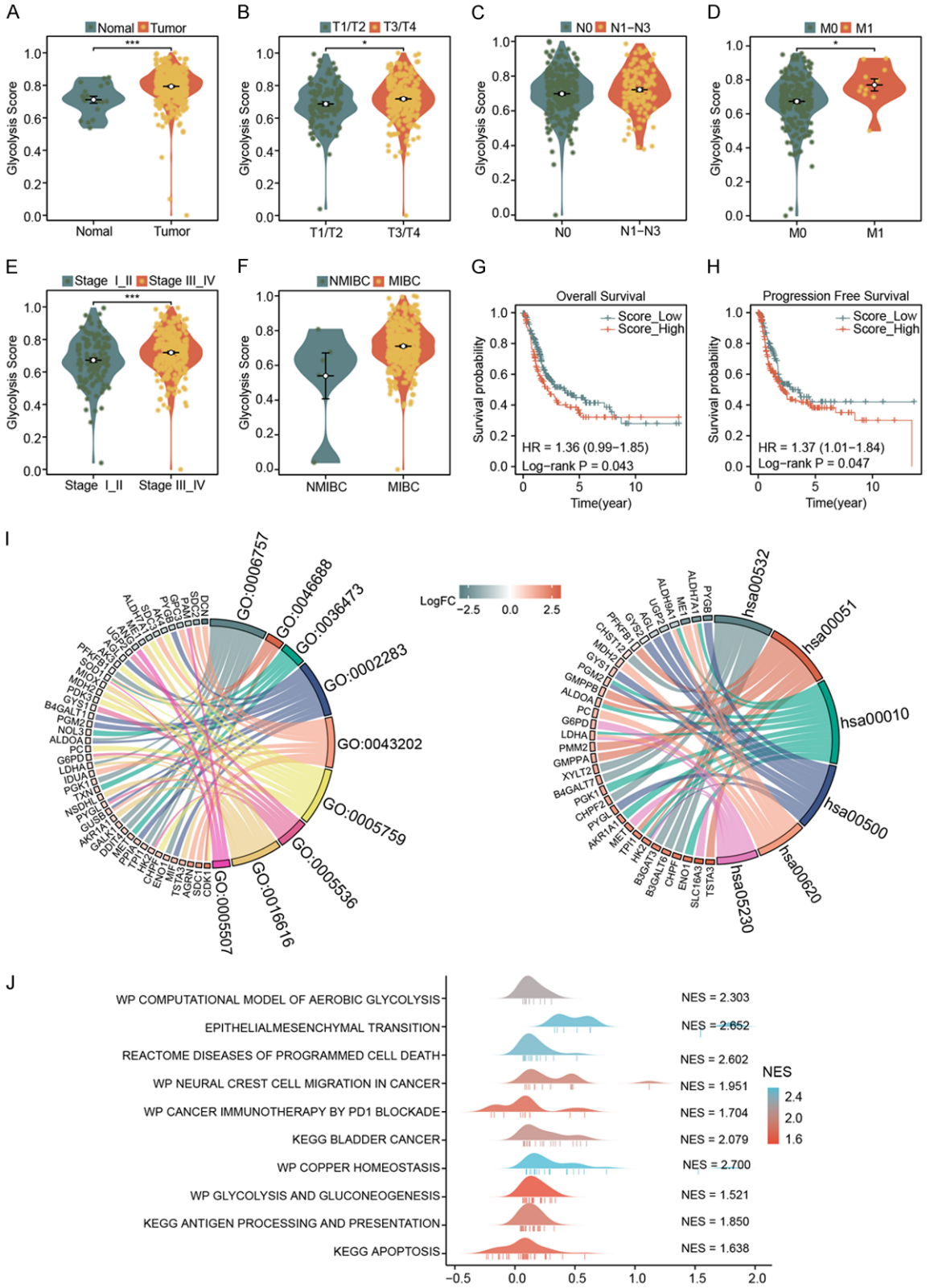

Figure 2. Differences, survival influence, and functional enrichment of glycolysis characteristic scores in BLCA. A. Differences in the glycolysis characteristic scores of BLCA tissue samples. B-F. Differences in the glycolysis characteristic scores of BLCA tissues classified according to TNM stage, staging system, and muscular infiltration. G. Kaplan-Meier estimates of overall survival according to the glycolysis score level. H. Kaplan-Meier estimates of progression-free survival according to the glycolysis score level. I. GO and KEGG analysis of glycolysis gene sets in

BLCA. J. GSEA analysis of glycolysis gene sets in BLCA. *P < 0.05, **P < 0.01, and ***P < 0.001. BLCA, bladder cancer; GO, Gene ontology; KEGG, Kyoto Encyclopedia of Genes and Genomes; GO:0006757, ATP generation from ADP; GO:0046688, response to copper ion; GO:0036473, cell death in response to oxidative stress; GO:0043202, lysosomal lumen; GO:0005759, mitochondrial matrix; GO:0005536, glucose binding; GO:0016616, oxidoreductase activity; GO:0005507, copper ion binding; hsa00532, Glycosaminoglycan biosynthesis; hsa00051, Fructose and mannose metabolism; hsa00010, Glycolysis/Gluconeogenesis; hsa00500, Starch and sucrose metabolism; hsa00620, Pyruvate metabolism; hsa05230, Central carbon metabolism in cancer.

central carbon metabolism in cancer, and other pathways (**Figure 2I**). Additionally, the TCGA-BLCA samples were grouped based on the Glycolysis-Scorehigh, and differentially expressed genes (DEGs) were extracted using GSEA. In addition to glycolysis, gluconeogenesis, and computational model of aerobic glycolysis, glycolysis gene sets were also involved in antigen processing and presentation, apoptosis, epithelial-mesenchymal transition, migration in cancer, bladder cancer, copper homeostasis, cancer immunotherapy by PD-1 blockade, and other signaling pathways (**Figure 2J**).

Identification of diagnostic markers of BLCA

The expression of 200 glycolysis-related genes between BLCA tissues and paracancerous tissues was compared to identify DEGs. Differential expression between the tissues was visualized as a heatmap, and DEGs were highlighted in a volcano plot (**Figure 3A**, **3B**). Based on the inclusion criteria of $|\log_2 FC| < 1$ and $P < 0.05$, a total of 50 glycolysis-related DEGs were obtained, with 34 induced and 16 repressed. Next, DEGs from the TCGA-BLCA dataset were analyzed by 3 machine learning algorithms: 14 DEGs, LASSO; 11 DEGs, SVM-RFE; and 19 DEGs, random forest (**Figure 3C-G**). These algorithms were also used to analyze DEGs from the GSE13507 dataset: 20 DEGs, LASSO; 18 DEGs, SVM-RFE; and 15 DEGs, random forest (**Figure 3H-L**). Finally, an intersection from both datasets was made with the 3 algorithms, and the *CHPF* gene was identified (**Figure 3M**). Its value in diagnosing BLCA was evaluated by generating a ROC curve (**Figure 3N**) and calculating its corresponding AUC. The AUC value of 0.811 showed *CHPF* had a satisfactory discriminative ability to recognize patients with BLCA.

Differences in CHPF expression between BLCA tissues and relevant correlation with clinical characteristics

We investigated *CHPF* differential expression between bladder cancer and adjacent tissues and revealed a significant increase in *CHPF* expression in cancer tissues (**Figure 4A**, $P < 0.001$). Furthermore, we assessed the correlation between *CHPF* expression and clinical features of BLCA. We revealed that *CHPF* expression was higher in T3 and T4 BLCA tissues than in T1 and T2 (**Figure 4B**, $P < 0.001$) and significantly elevated in stage III and IV BLCA tissues compared with stage I and II (**Figure 4E**, $P < 0.001$). Moreover, *CHPF* expression was significantly higher in tumor tissues with muscular invasion than in those without (**Figure 4F**, $P = 0.034$). Concerning tumor grade, *CHPF* expression also significantly rose in high-grade tumor tissues compared with the low (**Figure 4G**, $P = 0.036$). Regarding invasion, however, CHPF expression in BLCA tissues with lymph node or distant organ metastasis was unchanged in those without metastasis (**Figure 4C**, **4D**, $P > 0.05$). Finally, we evaluated the effect of *CHPF* expression on the survival of patients with BLCA and demonstrated that patients with bladder urothelial carcinoma with high *CHPF* expression had significantly decreased OS, PFS but unaffected disease-free survival rate (**Figure 4H-K**).

Correlation of CHPF expression with epithelial-to-mesenchymal transition (EMT) in BLCA

According to the GSEA analysis results, glycolysis genes correlated with migration in cancer, EMT, glycometabolism, immunotherapy, copper homeostasis, and other functions. Thus, the relationship between *CHPF* and each biological role was evaluated by separate experiments. Since abundant evidence shows EMT is the most crucial event in cancer metastasis, we investigated the association between *CHPF* expression and EMT-related markers. We discovered that the expression of 6 genes, *SNAI1*, *SNAI2*, *CDH2*, *FN1*, *TWIST1*, and *VIM*, was significantly higher in the high *CHPF* expression group than in the low (**Figure 5A**, $P < 0.001$), and each positively correlated with *CHPF* (**Figure 5B**, $P < 0.001$).

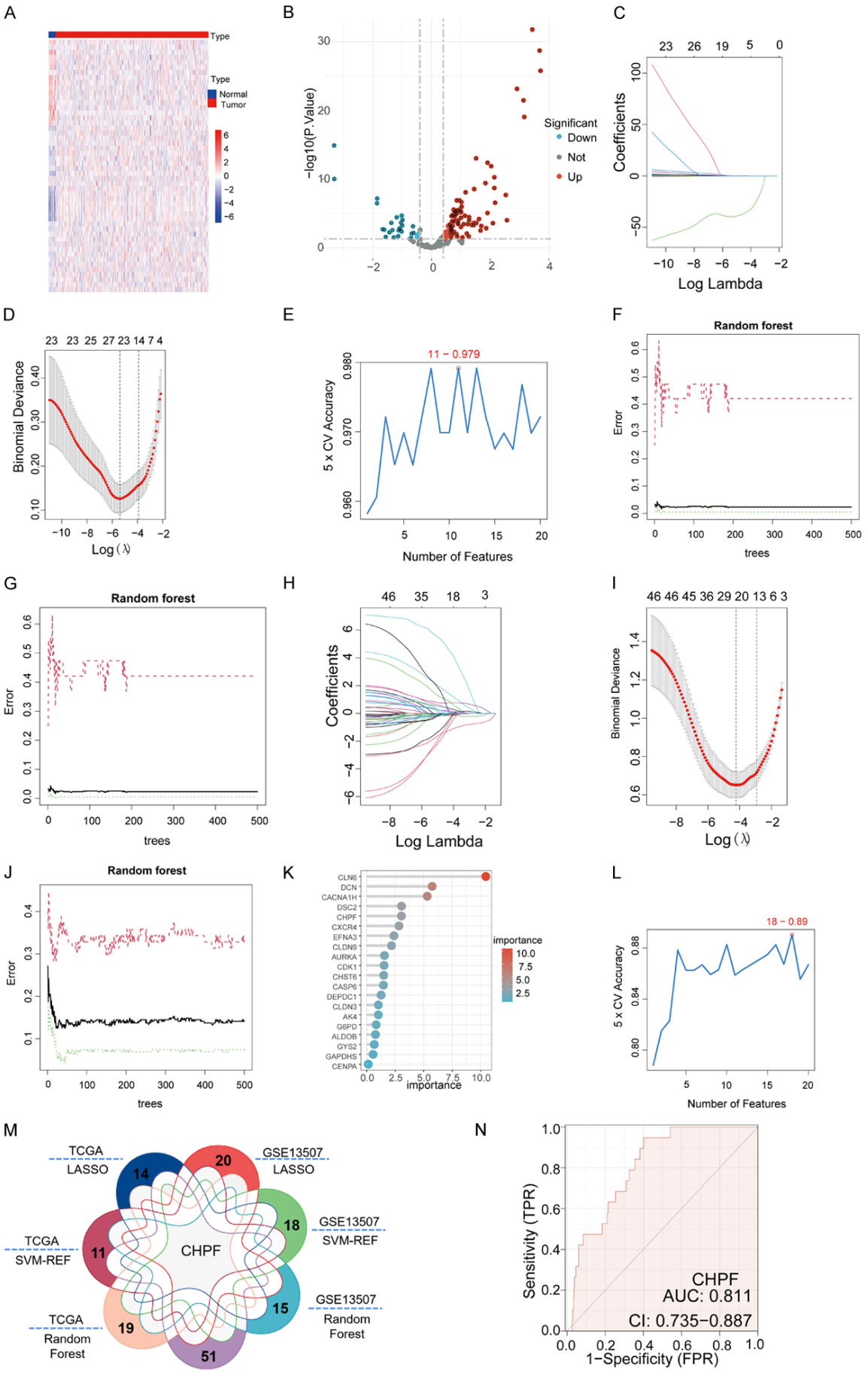
A
Type
Type
Normal
Tumor
B
−log10(P.Value)
Significant
Down
Not
Up
C
Coefficients
Log Lambda
D
Binomial Deviance
Log (λ)
E
11 − 0.979
5 x CV Accuracy
Number of Features
F
Random forest
Error
trees
G
Random forest
Error
trees
H
Coefficients
Log Lambda
I
Binomial Deviance
Log (λ)
J
Random forest
Error
trees
K
importance
L
18 − 0.89
5 x CV Accuracy
Number of Features
M
TCGA LASSO
GSE13507 LASSO
TCGA SVM-REF
GSE13507 SVM-REF
TCGA Random Forest
GSE13507 Random Forest
CHPF
14
20
11
18
19
15
51
N
Sensitivity (TPR)
1−Specificity (FPR)
CHPF
AUC: 0.811
CI: 0.735−0.887

Figure 3. Identification process of diagnostic markers for bladder cancer patients. A. Heatmap showing differential expression between BLCA and paracancerous tissues. The transition from blue to red signifies an increase in expression level. B. Volcano plot representing DEGs by significance and fold change. Red dots indicate up-regulated DEGs and green dots indicate down-regulated DEGs. C, D. The TCGA-BLCA dataset was searched using the LASSO regression method for the most distinctive genes. E. Screening the TCGA-BLCA-derived DEGs using the SVM-RFE algorithm. An analysis based on the RFE algorithm was done, followed by determining the statistical parameters of the most characteristic genes. F, G. The importance of each TCGA-BLCA-derived DEG was determined by the random forest algorithm. H, I. The GSE13507 dataset was analyzed using the LASSO regression method to identify the most distinctive genes. J, K. The random forest algorithm was used to determine the importance of each gene. L. Screening the GSE13507-derived DEGs with the SVM-RFE algorithm. An analysis was performed based on the RFE algorithm, followed by determining the statistical parameters of the most characteristic genes. M. The intersection of DEGs from both datasets obtained with the 3 machine learning algorithms. N. The ROC curve demonstrating the diagnostic value of the *CHPF* gene. FC, fold change; DEG, differentially expressed gene; AUC, area under the curve; CI, confidence interval; ROC, receiver operating characteristic; LASSO, least absolute shrinkage and selection operator; SVM-RFE, support vector machine recursive feature elimination.

Correlation of CHPF expression with glycolytic enzymes and transporters in BLCA

Among the glycolysis genes, 19 identified from published articles were related to glycolytic enzymes and transporters. The correlation of each gene with *CHPF* expression was explored using GSE13507, GSE176307, and TCGA-BLCA datasets, and the results were presented as a heatmap. A positive association between *CHPF* expression and 11 genes was uncovered in the 3 datasets, especially the GSE176307: *HK1*, *HK3*, *PFKP*, *PKM*, *LDHA*, *SLC2A1*, *3*, *4*, *5*, *SLC16A2*, and *3* (**Figure 6A**). The correlation was shown as a scatter plot for representative genes, such as hexokinase, phosphofructokinase, pyruvate kinase, lactate dehydrogenase, glucose transporter, and monocarboxylate transporter (**Figure 6C**). Next, TCGA-BLCA samples were divided into a high- and low-expression group according to *CHPF* expression. The differences in the expression of genes encoding glycolytic enzymes and transporters between the 2 groups were analyzed. The expression of 12 genes was lower in the low-expression group than in the high: *HK3*, *PFKP*, *PKM*, *LDHA*, *LDHB*, *SLC2A1*, *3*, *5*, *SLC16A1*, *2*, *3*, and *4* (**Figure 6B**, $P < 0.05$).

Correlation between CHPF expression and cuproptosis in BLCA

When in excess, intracellular copper directly binds lipid-acylated proteins of the TCA cycle. The binding results in protein aggregation and the loss of iron-sulfur clusters, elevating proteotoxic stress and inducing copper-dependent cell death. A total of 16 cuproptosis-related genes were collected from published articles, with *MTF1*, *GLS*, and *CDKN2A* inhibiting cuproptosis and the remaining 13 promoting it. Subsequently, the GSE13507, GSE176307, and TCGA-BLCA datasets were analyzed to explore the relationship between *CHPF* expression and each cuproptosis-related gene in BLCA. A negative correlation was observed between *CHPF* expression and that of 6 genes, *LIPT1*, *DLD*, *DLAT*, *PDHB*, and *ATP7A*, in all 3 datasets (**Figure 7A**, $P < 0.05$). Moreover, TCGA-BLCA samples were divided into the low and high groups according to the expression of CHPF. The differences in the expression of cuproptosis-related genes between the high- and low-*CHPF* expression groups were analyzed to identify changes in cuproptosis between the 2 groups (**Figure 7B**). The expression of 9 genes was up-regulated in the low-expression group versus the high: *LIPT1*, *LIAS*, *DLD*, *DBT*, *DLST*, *DLAT*, *PDHB*, *ATP7A*, and *MTF1* (**Figure 7B**, $P < 0.05$). Finally, *CHPF* was silenced in BLCA 5637 cells, and their DNA was analyzed with whole-genome sequencing. In the cells transfected with siRNA against *CHPF*, The expression of cuproptosis-promoting genes (e.g., *FDX1*) was significantly up-regulated after *CHPF* silencing in the cells transfected with siRNA against *CHPF* compared with those transfected with the negative control. By contrast, the expression of cuproptosis-inhibiting genes (e.g., *CDKN2A*) was down-regulated (**Figure 7C**).

Relationship between CHPF expression and immune cell infiltration in BLCA

The correlation of *CHPF* expression with BLCA immune microenvironment and immune cell infiltration was examined. First, the influence of *CHPF* expression on the immune microenvironment in the TCGA-BLCA, GSE13507, and

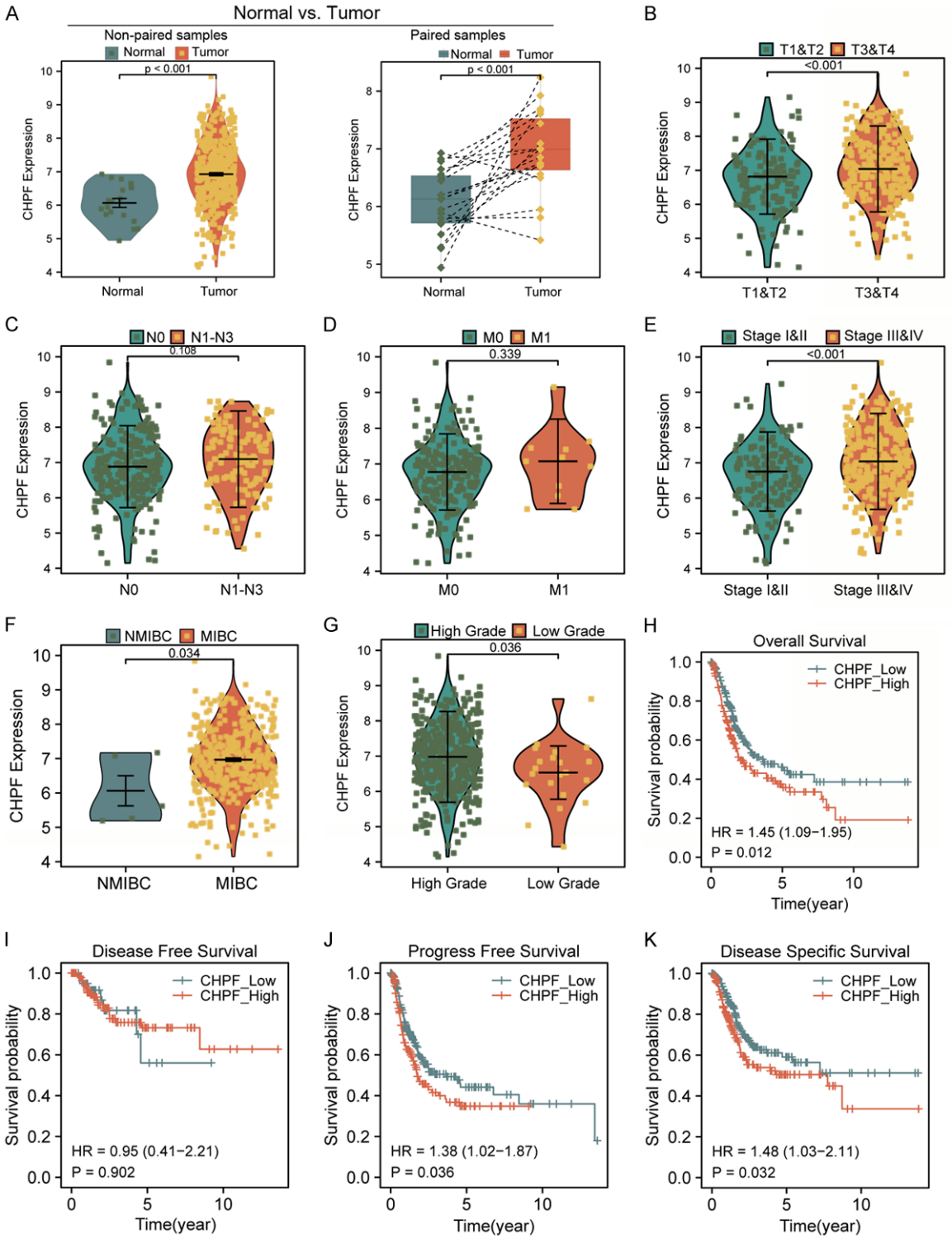

Figure 4. Differences in the expression of CHPF between BLCA and relevant correlation with clinical characteristics. A. *CHPF* expression was significantly up-regulated in BLCA tissues compared with adjacent tissues, as shown by unpaired and paired *t* tests of 19 pairs of BLCA and matched adjacent noncancerous tissue. B. *CHPF* expression was significantly higher in tissues with the T3-T4 category than in T1-T2. C. *CHPF* had higher expression in tissues with the N1-N3 category than those with N0. D. *CHPF* expression was higher in tissues with the M1 category than in those with M0. E. *CHPF* expression was significantly higher in stage III and IV tumor tissues than in stages I and II. F. *CHPF* expression was significantly higher in tissues with muscle invasion than in those without. G. *CHPF* expression was significantly higher in high-grade tumor tissues than in low-grade ones. H-K. The impact of *CHPF* expression on overall, disease-free, progression-free, and disease-specific survival in patients with BLCA.

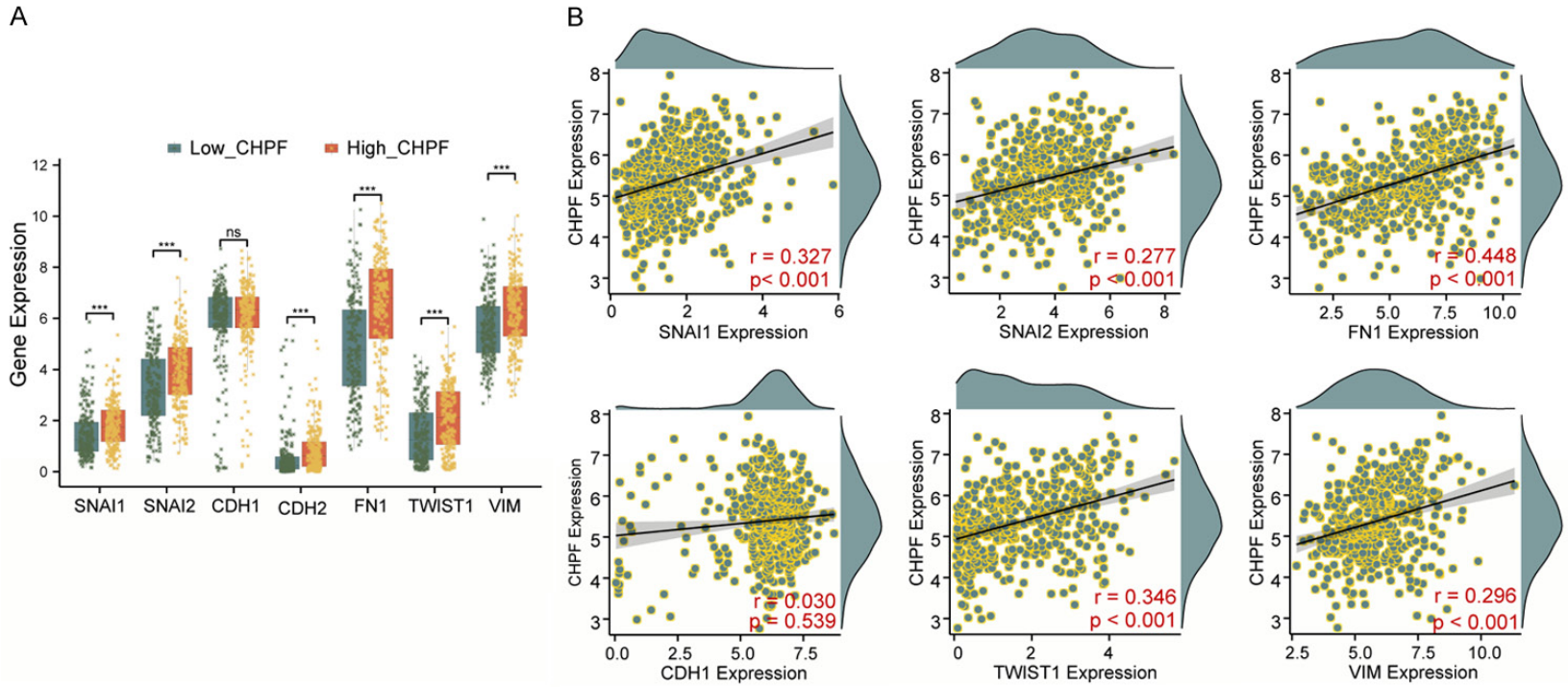

Figure 5. Analysis of EMT-associated markers in BLCA. A. Variations in EMT marker expression between sample groups with high and low *CHPF* expression. B. Correlation between *CHPF* and EMT marker expression depicted as a scatter plot. *np > 0.05, ***P < 0.001.

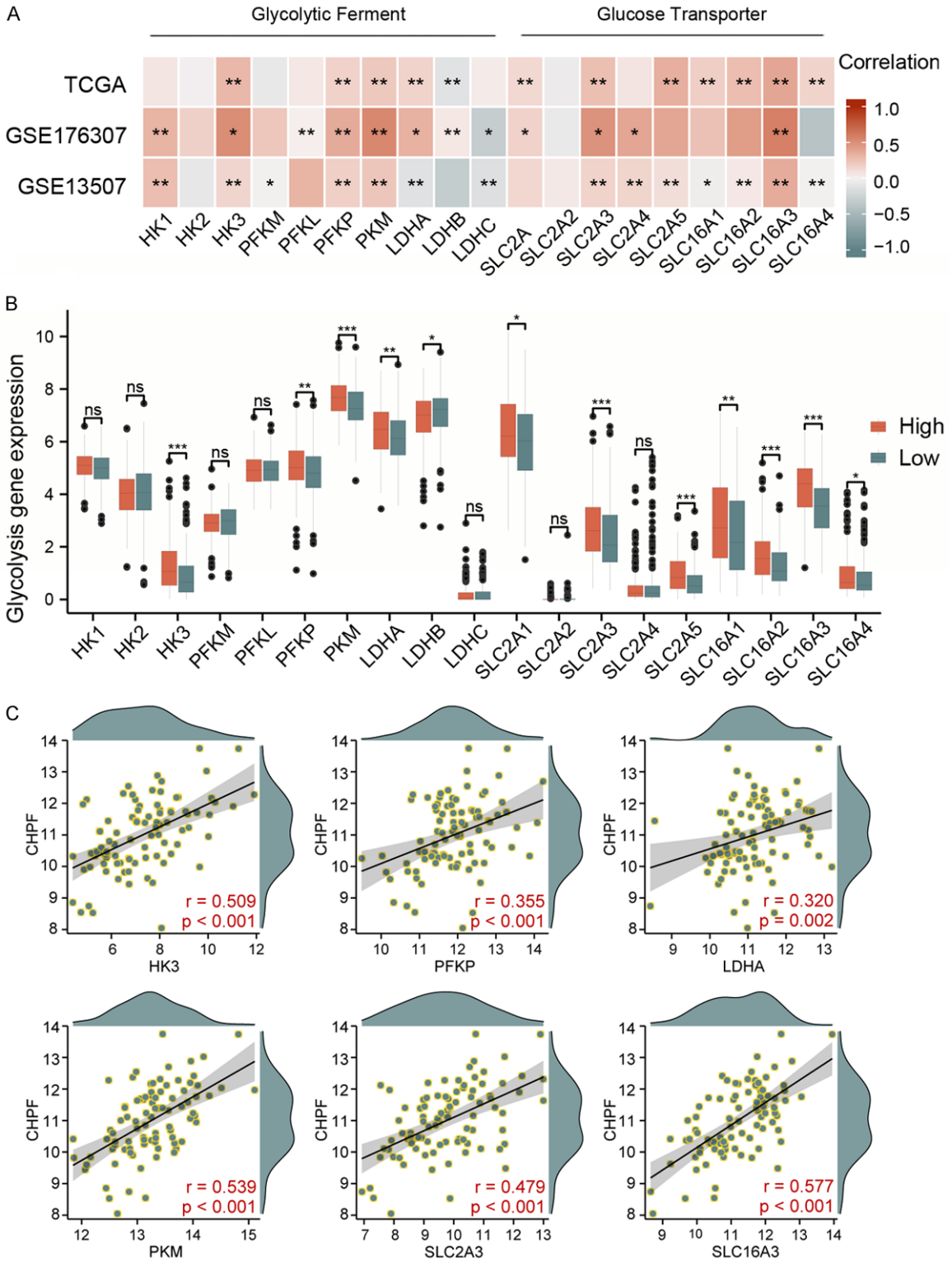

Figure 6. Correlation of CHPF expression with glycolytic enzymes and transporters in BLCA. A. Correlation of *CHPF* expression in BLCA with the expression of glycolytic enzymes and transporters in the TCGA-BLCA, GSE176307, and GSE13507 datasets. B. Variations in the expression of glycolysis-related genes between samples with high and low *CHPF* expression. C. Correlation between *CHPF* expression and that of 6 glycolysis-related genes (HK3, PFKP, PKM, SLC2A3, SLC16A2, and SLC16A3) shown as a scatter plot. **P* < 0.05, ***P* < 0.01, and ****P* < 0.001.

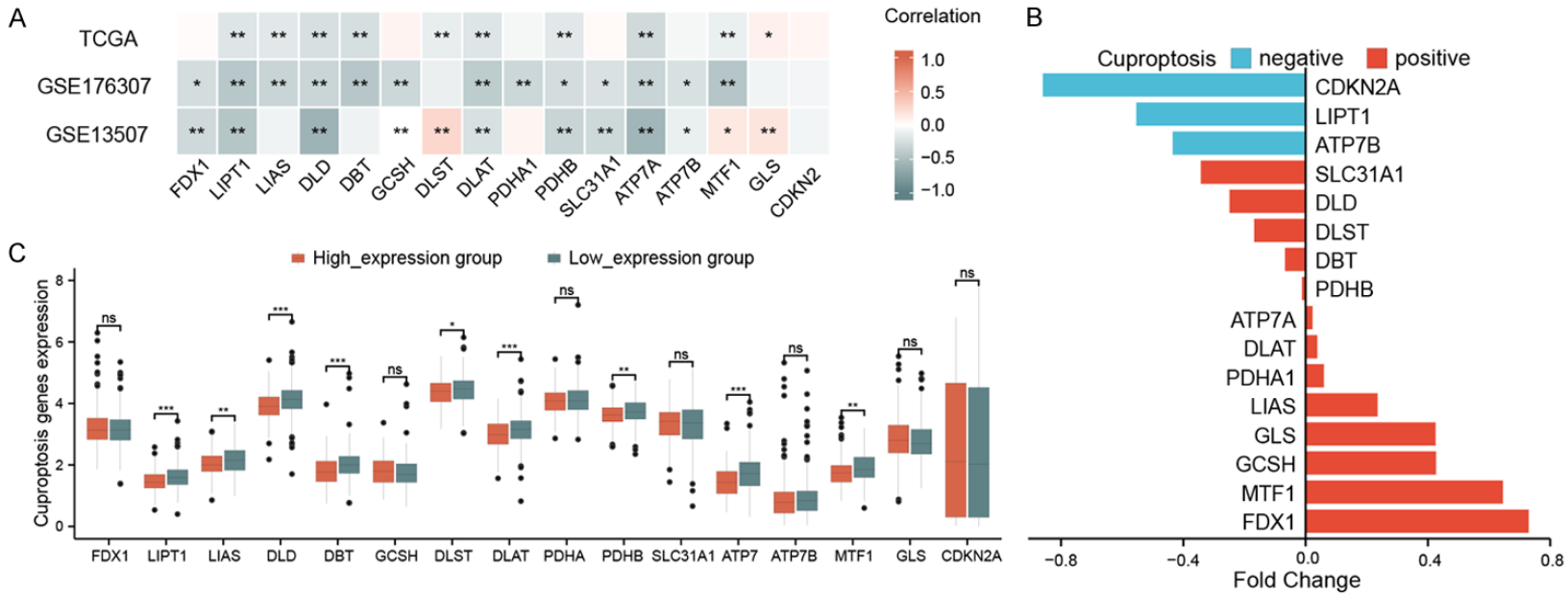

Figure 7. CHPF expression is associated with cuproptosis-related genes in BLCA. A. Positive correlation between *CHPF* and cuproptosis-related gene expression in BLCA discovered by analyzing the TCGA-BLCA, GSE176307, and GSE13507 datasets. B. Expression differences of cuproptosis-related genes in BLCA samples from patients with high or low *CHPF* expression. C. Sequencing data of the 5637 BLCA cell line revealing changes in the expression of cuproptosis-related genes following *CHPF* knockdown. $*P < 0.05$, $**P < 0.01$, and $***P < 0.001$.

GSE176307 datasets was assessed with the ESTIMATE algorithm. The results demonstrated that the interstitial cell, immune cell, and ESTIMATE scores in the high *CHPF* expression group significantly increased, suggesting low tumor purity (**Figure 8A-C**). Subsequently, the infiltration scores of 27 immune cells in TCGA-BLCA tumor samples were quantified by the ssGSEA algorithm. The infiltration level of 25 immune cells in the overexpression subsets of *CHPF* increased significantly, with neutrophils, activated B cells, regulatory T cells, and macrophages having the highest fold changes (**Figure 8D**). Analyzing the sequencing data of 5637 BLCA cells revealed that the immune infiltration levels of activated B, regulatory T, and activated $CD4^+$ T cells decreased significantly after *CHPF* silencing (**Figure 8D**).

Influence of CHPF on drug sensitivity in targeted therapy and immunotherapy

We retrieved the immunotherapy data of the GSE176307 and IMvigor 210 datasets and investigated the correlation between *CHPF* expression and immunotherapy responses and the relevant influence on patient prognosis. Analyzing the immunotherapy data in the GSE176307, we found that *CHPF* expression in the patients from the non-progression group was lower than in those from the progression group (**Figure 8E**, $P = 0.73$). We also discovered that high *CHPF* expression was a risk factor for the PFS of patients after immunotherapy (**Figure 8E**, $P < 0.05$). Furthermore, searching immunotherapy data in the IMvigor210 dataset, we observed *CHPF* expression in the patients from the treatment response group was lower than in those from the non-response one (**Figure 8F**, $P = 0.19$). Similarly, high *CHPF* expression was a risk factor for the OS of patients after immunotherapy (**Figure 8F**, $P < 0.05$).

Influence of CHPF on drug sensitivity in targeted therapy

Targeted drugs play a crucial role in tumor treatment, and the changes in tumor-specific genes are associated with the response to targeted therapy. Because effective biomarkers are lacking for targeted therapy, whether *CHPF* expression relates to drug sensitivity was evaluated. A positive association was discovered between *CHPF* expression and the sensitivity of 5 inhibitors: AKT, B-RAF, MET, PI3K, and mTORC. Conversely, a negative correlation was found with the sensitivity of EGFR inhibitors. These findings indicate *CHPF* may become an index for predicting the efficacy of the before mentioned drug therapy (**Figure 9**).

Correlation between CHPF expression and clinical characteristics and FDG uptake in BLCA

To further verify the accuracy of prediction results in the previous subtitle, BLCA tissues were analyzed with IHC staining to detect CHPF protein expression in tumor and adjacent tissues. A total of 33 BLCA tissue samples and 8 paired paracancerous tissue samples were stained and scored by 2 qualified pathologists. Subsequently, the correlation between the *CHPF* IHC score (H-score) and the clinical characteristics of patients with BLCA patients was analyzed. The CHPF protein was mainly expressed in the cytoplasm of BLCA cells, and its levels were higher in BLCA tissues than in the paired paracancerous. A significant difference in the H-score between both types of tissue samples was observed (**Figure 10A**). In addition, CHPF expression in invasive, muscular invasive, and high-grade tumors was significantly up-regulated, and the scores statistically differed (**Figure 10A**). Similarly, CHPF expression was higher in advanced tumors based on the T category (**Figure 10B**). Finally, the PET/CT data of 17 patients with BLCA were collected, and the correlation between CHPF expression and FDG uptake was analyzed. The CHPF protein expression was significantly up-regulated in BLCA tissues with higher FDG uptake and positively correlated with FDG uptake in BLCA tissues (**Figure 10C**, **10D**).

Discussion

Aerobic glycolysis is a unique metabolic strategy utilized by tumor cells that allows continuous proliferation of tumor cells and accelerates their progression. Hence, aerobic glycolysis can be considered a marker of cancer [19]. Pancreatic cancer, glioma, and oral cancer cells become more invasive under aerobic glycolysis, promoting them to evade immune surveillance [20, 21]. Evidence shows glycolysis is a crucial factor in BLCA progression, and genes that control glycolytic steps represent a promising therapeutic target [22, 23]. Here, we utilized the ssGSEA algorithm to evaluate the

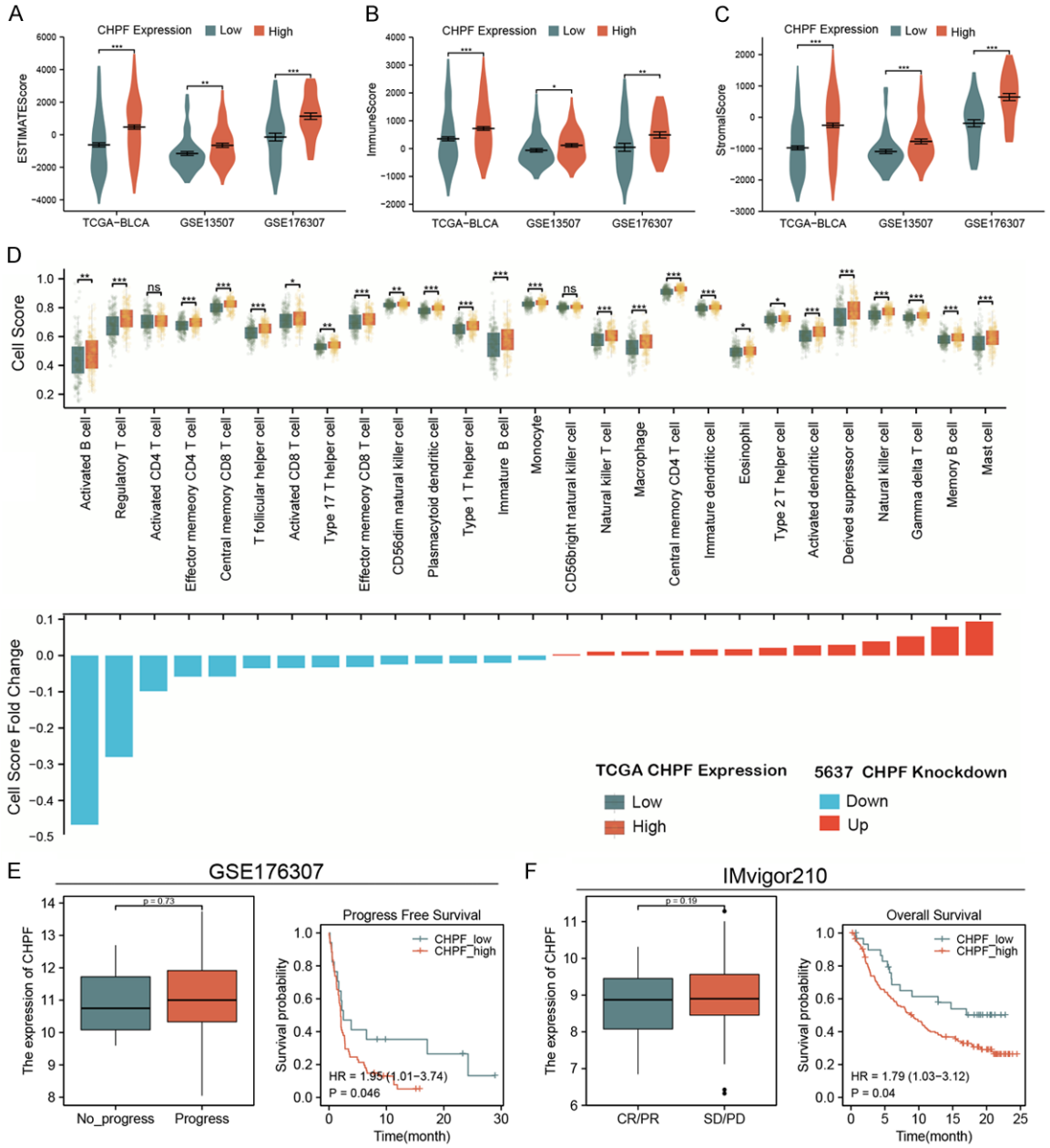

Figure 8. Correlation between CHPF expression and immune microenvironment, immune cell infiltration, and immunotherapy in BLCA. A-C. Differences in the stromal, immune, and ESTIMATE scores between high- and low-*CHPF* expression groups in BLCA based on the analysis of TCGA-BLCA, GSE176307, and GSE13507 datasets. D. Differences in the immune cell infiltration score between the high and low-*CHPF* expression groups based on the TCGA-BLCA dataset and changes in the immune cell infiltration score of the 5637 BLCA cell line sequencing data after *CHPF* silencing. E. Differences in *CHPF* expression between the non-progression and progression groups based on the GSE176307 dataset. Kaplan-Meier estimates for PFS according to *CHPF* expression are shown. F. Differences in *CHPF* expression between the treatment response and non-response groups based on the IMvigor 210 dataset. Kaplan-Meier estimates for OS according to *CHPF* expression are indicated. **P* < 0.05, ***P* < 0.01, and ****P* < 0.001. PFS, progression-free survival; OS, overall survival.

glycolysis feature score of RNA-sequenced tissue samples from the public TCGA-BLCA dataset. We observed a significantly higher score in BLCA tissues than in adjacent tissues. We also explored the influence of glycolysis feature scores on clinical characteristics and prognosis of BLCA. We revealed that patients with higher scores had more advanced pathological stages

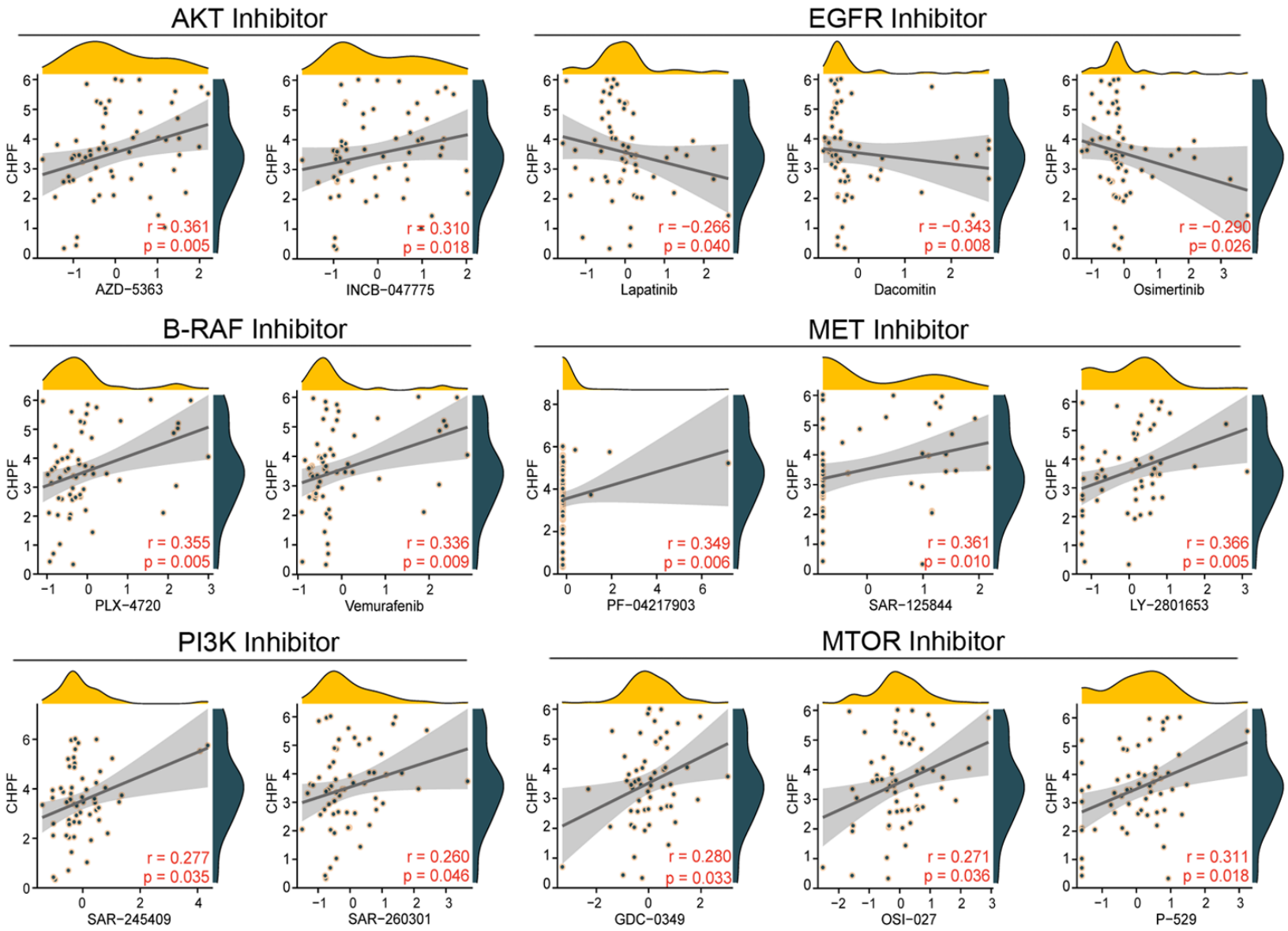

Figure 9. The correlation-related scatter plot between CHPF and targeted drug sensitivity.

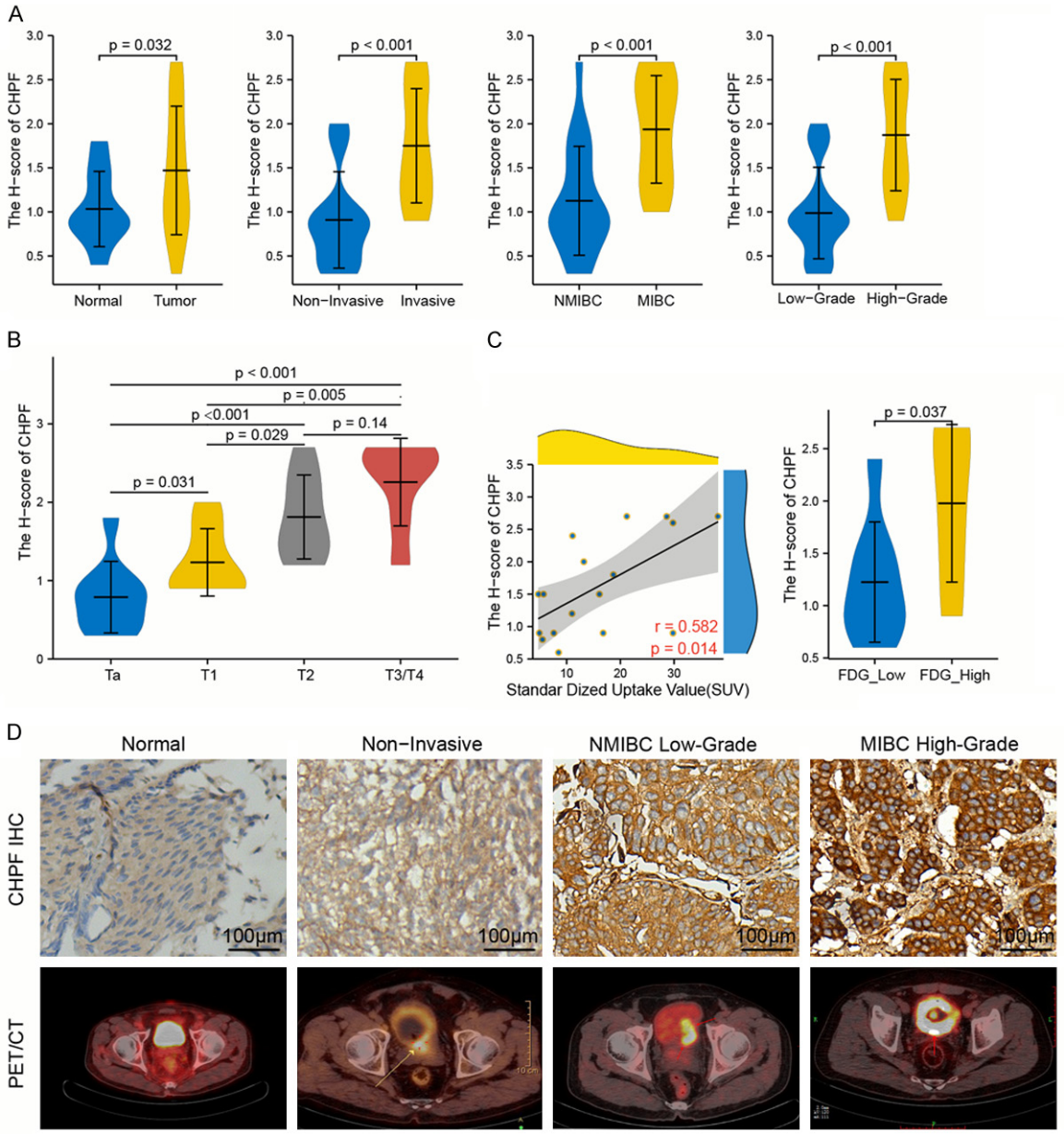

Figure 10. Correlation between CHPF expression and clinical characteristics and FDG uptake in BLCA. A. Differences in H score between 2 groups: BLCA vs. paracancerous tissues; non-invasive vs. invasive tumors; non-muscular invasive bladder cancer (NMIBC) vs. muscular invasive bladder cancer (MIBC); and low-grade vs. high-grade tumors. B. Differences in *CHPF* expression between different T category BLCA tissues. C. Representative PET/CT and *CHPF* IHC images of patients with BLCA with high or low FDG uptake. C. Correlation between FDG uptake and *CHPF* expression in 17 patients with BLCA. The differences in *CHPF* expression between patients with high or low FDG uptake. D. Immunohistochemical stains of *CHPF* and PET/CT images of patients BLCA with different pathological features.

of the tumor and were more prone to distant metastasis, lymph node metastasis, and tumor invasion into the muscularis propria. Moreover, a high glycolysis feature score is a risk factor for the OS and PFS of the patients. Increased expression of pyruvate dehydrogenase kinase 1 (*PDK1*), one of the primary regulators of glycometabolism, is an independent predictive factor for the OS of patients with invasive bladder cancer, consistent with our findings [24].

The potential functions of glycolysis genes and those central to BLCA were also examined. After screening 200 genes in the glycolysis

gene set, we found significant differences in the expression of 50 genes. The enrichment analyses uncovered that these genes were mainly involved in signaling pathways, such as glycometabolism, immunotherapy, and copper homeostasis. Subsequently, we constructed a model related to these 50 DEGs from 2 datasets using 3 machine learning methods. We showed that the chondroitin polymerization factor (*CHPF*) gene had the most significant diagnostic value for BLCA. This gene encodes a 775-amino acid type II transmembrane protein composed that assists in the extension of chondroitin sulfate through a potential N-glycosylation site and 3'-untranslated region. Hence, it has a considerable role in chondroitin sulfate biosynthesis [25, 26]. Evidence indicates *CHPF* is overexpressed in many tumors, such as colon cancer, breast cancer, and melanoma, and is related to tumor metastasis and survival time [27, 28]. Because it is a recently discovered tumor-related gene, *CHPF* has not yet been comprehensively analyzed in BLCA. Our study reveals that *CHPF* is highly expressed in BLCA tissues and that its up-regulation is associated with higher pathological grades and advanced clinical stages, rendering it a risk factor for OS, PFS, and DSS in patients with BLCA. These findings are consistent with the cancer-promoting effect *CHPF* exerts in many other common tumors.

The phenotypic transformation of epithelial cells into mesenchymal, or EMT, is closely associated with the development and spread of cancer. High SNAI1 and VIM expression promote EMT and metastasis in BLCA tissues, making these proteins recognized markers of EMT [29]. We discovered that glycolytic gene sets enhanced tumor migration and the expression of *SNAI1* and *VIM* EMT markers. These markers were significantly induced in the tissues with high *CHPF* expression and positively correlated with *CHPF,* suggesting *CHPF* could be used as a marker of metastatic risk in bladder BLCA.

Hexokinase, phosphofructokinase, and pyruvate kinase are essential enzymes in the glycolytic pathway that significantly contribute to glycolysis metabolism. The increased expression of these enzymes and transporter proteins stimulates glycolysis, conferring tumor cell proliferation and chemotherapy resistance in various malignant neoplasms, such as bladder, breast, ovarian, and lung cancers [30-34]. The overexpression of glucose transporter genes *SLC2A* and *SLC16A* promotes glycolysis, enhances glucose uptake, and accelerates tumor cell growth [35, 36]. Our correlation analyses of 3 different datasets showed a positive association between the expression of *CHPF* and glycolytic enzymes and transporters in BLCA tissues. These findings imply that *CHPF* works with glycolytic enzymes and transporters to promote glycolysis in BLCA cells.

Copper is an essential trace element involved in numerous vital processes, and its homeostasis participates in the proliferation, angiogenesis, and metastasis of cancer cells [37, 38]. When in excess, it directly binds fatty acylated proteins of the TCA cycle, triggering protein aggregation, the loss of iron-sulfur complexes, and copper-dependent cell death [39]. We evaluated the effect of *CHPF* expression on cuproptosis-related genes using the 3 datasets. We found that *CHPF* was negatively linked with *DLD*, *DLAT*, *PDHB*, and *ATP7A* cuproptosis-related genes in BLCA tissues. Moreover, these genes and 5 other cuproptosis-associated genes (*LIPT1*, *LIAS*, *DBT*, *DLST*, and *MTF1*) were up-regulated in the tumor tissues with low *CHPF* expression. Silencing *CHPF* in BLCA cells confirmed this relationship, showing cuproptosis-promoting genes (e.g., *FDX1*) are up-regulated, and cuproptosis-inhibiting genes (e.g., *CDKN2A*) are down-regulated. This link between *CHPF* and cuproptosis in BLCA has never been described and should provide a basis for further exploration of cuproptosis in this disease.

The tumor immune microenvironment and immune cell infiltration levels affect the metastasis and prognosis of patients with BLCA [40, 41]. We investigated the correlation between *CHPF* and the BLCA microenvironment using the 3 BLCA datasets. We showed that the interstitial cell, immune cell, and ESTIMATE scores and the infiltration levels of 25 immune cells significantly increased in BLCA tissues with higher *CHPF* expression, especially in neutrophils, activated B cells, regulatory T cells, and macrophages. Moreover, the genomic sequencing data of the BLCA cell line revealed that the immune infiltration levels of immune cells, such as activated B and regulatory T cells, decreased significantly after *CHPF* silencing. This observation indicates that *CHPF* influenc-

es the immunological response of BLCA by altering the expression of B and T cells.

Tumor-infiltrating immune cells (e.g., regulatory T cells) are effectors of immunotherapy, and targeted regulation of tumor immune cell infiltration is a promising strategy for cancer treatment [42-44]. Since our findings indicated that *CHPF* expression is closely related to immune cell infiltration, we sought to identify whether *CHPF* affects the immunotherapeutic response in BLCA by regulating the expression of immune cell infiltration. The expression of *CHPF* did not change between the 2 analyzed immunotherapy datasets. Nonetheless, the effect of *CHPF* expression on the OS and PFS of patients was significantly different following immunotherapy. Why *CHPF* expression was unaffected may be the small number of study cohorts included in this study, which would require expanding the cohorts to explore *CHPF* expression under immunotherapy.

Targeted therapy based on the PI3K/AKT/mTOR and fibroblast growth factor receptor (FGFR) signaling pathways have achieved favorable outcomes in treating some tumors, including BLCA. The gene changes related to these pathways are associated with the response to targeted therapy [44, 45]. Thus, we explored the influence of *CHPF* expression on drug sensitivity in targeted therapy. We uncovered a positive correlation between *CHPF* and the sensitivity of 5 inhibitor drugs (AKT, B-RAF, MET, PI3K, and mTORC) and a negative correlation with the sensitivity of EGFR inhibitors. This finding suggests that *CHPF* is a potential biomarker for predicting the sensitivity of these drugs in targeted therapy.

We also verified the bioinformatics results by IHC staining of BLCA tissues. We demonstrated that the CHPF protein was mainly expressed in the cytoplasm of BLCA cells and showed that its levels in BLCA tissues were significantly higher than in paracancerous tissues, consistent with the bioinformatics data. We also revealed that ^{18}F-FDG uptake positively correlated with CHPF protein expression in patients with BLCA. Thus, CHPF may enhance the glycolytic ability in patients by promoting the activity of key glycolytic enzymes, enhancing BLCA occurrence and progression.

Although our study offers valuable novel insights, it has some limitations. First, it used bioinformatics approaches, which suggests the preliminary nature of the findings. Second, the number of samples analyzed with immunohistochemistry is small, and the clinicopathological features covered are relatively limited. Therefore, future research should focus on collecting more clinical data to verify the effect of *CHPF* on immunotherapy and patient survival and to explore the mechanism of this gene in BLCA more comprehensively.

In conclusion, glycolysis-associated gene *CHPF* is overexpressed in BLCA. Its expression is related to the clinical characteristics and prognosis of patients with BLCA. In addition, it is involved in many cellular and tumor-related processes in BLCA tissues, such as EMT, glycolysis, immune cell infiltration, and cuproptosis. It also has a satisfactory value in diagnosing BLCA and positively correlates with the sensitivity of inhibitor drugs. Thus, *CHPF* is a biomarker for the diagnosis of BLCA and a valuable potential target for treating the disease.

Acknowledgements

This work was supported by the National Natural Science Foundation of China (No. 82060276). The National Natural Science Foundation of China (Number: 82060462), The Science and Technology Foundation of Guizhou Province (Number: [2020]1Y303), Science and Technology Plan project of Guizhou Province (Number: [2019]5405), Foundation of Health and Family Planning Commission of Guizhou Province (Number: gzwjkj2019-1-127) and the Doctoral Foundation of Guizhou Provincial People's Hospital (GZSYBS[2018]02).

All participants signed written informed consent.

Disclosure of conflict of interest

None.

Address correspondence to: Dr. Fa Sun, Guizhou Medical University, No. 9 Beijing Road, Yunyan District, Guiyang 550001, Guizhou, China. Tel: +86-15185125266; E-mail: sfgmc@sina.com

References

[1] Bray F, Ferlay J, Soerjomataram I, Siegel RL, Torre LA and Jemal A. Global cancer statistics 2018: GLOBOCAN estimates of incidence and mortality worldwide for 36 cancers in 185

countries. CA Cancer J Clin 2018; 68: 394-424.
[2] Lenis AT, Lec PM, Chamie K and Mshs MD. Bladder cancer: a review. JAMA 2020; 324: 1980-1991.
[3] Sun M and Trinh QD. Diagnosis and staging of bladder cancer. Hematol Oncol Clin North Am 2015; 29: 205-218, vii.
[4] Babjuk M, Bohle A, Burger M, Capoun O, Cohen D, Comperat EM, Hernandez V, Kaasinen E, Palou J, Roupret M, van Rhijn BWG, Shariat SF, Soukup V, Sylvester RJ and Zigeuner R. EAU guidelines on non-muscle-invasive urothelial carcinoma of the bladder: update 2016. Eur Urol 2017; 71: 447-461.
[5] Ritch CR, Velasquez MC, Kwon D, Becerra MF, Soodana-Prakash N, Atluri VS, Almengo K, Alameddine M, Kineish O, Kava BR, Punnen S, Parekh DJ and Gonzalgo ML. Use and validation of the AUA/SUO Risk Grouping for non-muscle invasive bladder cancer in a contemporary cohort. J Urol 2020; 203: 505-511.
[6] Zhou Z, Zhang Z, Chen H, Bao W, Kuang X, Zhou P, Gao Z, Li D, Xie X, Yang C, Chen X, Pan J, Tang R, Feng Z, Zhou L, Wang L, Yang J and Jiang L. SBSN drives bladder cancer metastasis via EGFR/SRC/STAT3 signalling. Br J Cancer 2022; 127: 211-222.
[7] Hargadon KM, Johnson CE and Williams CJ. Immune checkpoint blockade therapy for cancer: an overview of FDA-approved immune checkpoint inhibitors. Int Immunopharmacol 2018; 62: 29-39.
[8] Zappasodi R, Merghoub T and Wolchok JD. Emerging concepts for immune checkpoint blockade-based combination therapies. Cancer Cell 2018; 33: 581-598.
[9] Warburg O. On the origin of cancer cells. Science 1956; 123: 309-314.
[10] Li W, Xu M, Li Y, Huang Z, Zhou J, Zhao Q, Le K, Dong F, Wan C and Yi P. Comprehensive analysis of the association between tumor glycolysis and immune/inflammation function in breast cancer. J Transl Med 2020; 18: 92.
[11] Xu K, Yin N, Peng M, Stamatiades EG, Shyu A, Li P, Zhang X, Do MH, Wang Z, Capistrano KJ, Chou C, Levine AG, Rudensky AY and Li MO. Glycolysis fuels phosphoinositide 3-kinase signaling to bolster T cell immunity. Science 2021; 371: 405-410.
[12] Ogawa H, Shionyu M, Sugiura N, Hatano S, Nagai N, Kubota Y, Nishiwaki K, Sato T, Gotoh M, Narimatsu H, Shimizu K, Kimata K and Watanabe H. Chondroitin sulfate synthase-2/chondroitin polymerizing factor has two variants with distinct function. J Biol Chem 2010; 285: 34155-34167.
[13] Lin X, Han T, Xia Q, Cui J, Zhuo M, Liang Y, Su W, Wang L, Wang L, Liu Z and Xiao X. CHPF promotes gastric cancer tumorigenesis through the activation of E2F1. Cell Death Dis 2021; 12: 876.
[14] Hou XM, Baloch Z, Zheng ZH, Zhang WH, Feng Y, Li DD, Wu XA and Yang SH. Knockdown of CHPF suppresses cell progression of non-small-cell lung cancer. Cancer Manag Res 2019; 11: 3275-3283.
[15] Liu CH, Wu BR, Ho YJ, Chu YH, Hsu WC, Tseng TJ, Li JP and Liao WC. CHPF regulates the aggressive phenotypes of hepatocellular carcinoma cells via the modulation of the decorin and TGF-β pathways. Cancers (Basel) 2021; 13: 1261.
[16] Tang D, Chen X and Kroemer G. Cuproptosis: a copper-triggered modality of mitochondrial cell death. Cell Res 2022; 32: 417-418.
[17] Wang Y, Zhang L and Zhou F. Cuproptosis: a new form of programmed cell death. Cell Mol Immunol 2022; 19: 867-868.
[18] Bai Y, Zhang Q, Liu F and Quan J. A novel cuproptosis-related lncRNA signature predicts the prognosis and immune landscape in bladder cancer. Front Immunol 2022; 13: 1027449.
[19] Hanahan D and Weinberg RA. Hallmarks of cancer: the next generation. Cell 2011; 144: 646-674.
[20] Hu Q, Qin Y, Ji S, Xu W, Liu W, Sun Q, Zhang Z, Liu M, Ni Q, Yu X and Xu X. UHRF1 promotes aerobic glycolysis and proliferation via suppression of SIRT4 in pancreatic cancer. Cancer Lett 2019; 452: 226-236.
[21] Sur S, Nakanishi H, Flaveny C, Ippolito JE, McHowat J, Ford DA and Ray RB. Inhibition of the key metabolic pathways, glycolysis and lipogenesis, of oral cancer by bitter melon extract. Cell Commun Signal 2019; 17: 131.
[22] Che K, Han W, Li D, Cui S, Zhang M, Yang X and Niu H. Correlations between glycolysis with clinical traits and immune function in bladder urothelial carcinoma. Biosci Rep 2021; 41: BSR20203982.
[23] Huber K, Mestres-Arenas A, Fajas L and Leal-Esteban LC. The multifaceted role of cell cycle regulators in the coordination of growth and metabolism. FEBS J 2021; 288: 3813-3833.
[24] Zhu J, Zheng G, Xu H, Jin X, Tang T and Wang X. Expression and prognostic significance of pyruvate dehydrogenase kinase 1 in bladder urothelial carcinoma. Virchows Arch 2020; 477: 637-649.
[25] Yada T, Gotoh M, Sato T, Shionyu M, Go M, Kaseyama H, Iwasaki H, Kikuchi N, Kwon YD, Togayachi A, Kudo T, Watanabe H, Narimatsu H and Kimata K. Chondroitin sulfate synthase-2. Molecular cloning and characterization of a novel human glycosyltransferase homologous to chondroitin sulfate glucuronyltransferase, which has dual enzymatic activities. J Biol Chem 2003; 278: 30235-30247.

[26] Izumikawa T, Koike T, Shiozawa S, Sugahara K, Tamura J and Kitagawa H. Identification of chondroitin sulfate glucuronyltransferase as chondroitin synthase-3 involved in chondroitin polymerization: chondroitin polymerization is achieved by multiple enzyme complexes consisting of chondroitin synthase family members. J Biol Chem 2008; 283: 11396-11406.
[27] Wu ZY, He YQ, Wang TM, Yang DW, Li DH, Deng CM, Cao LJ, Zhang JB, Xue WQ and Jia WH. Glycogenes in oncofetal chondroitin sulfate biosynthesis are differently expressed and correlated with immune response in placenta and colorectal cancer. Front Cell Dev Biol 2021; 9: 763875.
[28] Liao WC, Yen HR, Chen CH, Chu YH, Song YC, Tseng TJ and Liu CH. CHPF promotes malignancy of breast cancer cells by modifying syndecan-4 and the tumor microenvironment. Am J Cancer Res 2021; 11: 812-826.
[29] Monteiro-Reis S, Miranda-Goncalves V, Guimaraes-Teixeira C, Martins-Lima C, Lobo J, Montezuma D, Dias PC, Neyret-Kahn H, Bernard-Pierrot I, Henrique R and Jeronimo C. Vimentin epigenetic deregulation in bladder cancer associates with acquisition of invasive and metastatic phenotype through epithelial-to-mesenchymal transition. Int J Biol Sci 2023; 19: 1-12.
[30] Pajak B, Siwiak E, Sołtyka M, Priebe A, Zieliński R, Fokt I, Ziemniak M, Jaśkiewicz A, Borowski R, Domoradzki T and Priebe W. 2-deoxy-D-glucose and its analogs: from diagnostic to therapeutic agents. Int J Mol Sci 2019; 21: 234.
[31] Raez LE, Papadopoulos K, Ricart AD, Chiorean EG, Dipaola RS, Stein MN, Rocha Lima CM, Schlesselman JJ, Tolba K, Langmuir VK, Kroll S, Jung DT, Kurtoglu M, Rosenblatt J and Lampidis TJ. A phase I dose-escalation trial of 2-deoxy-D-glucose alone or combined with docetaxel in patients with advanced solid tumors. Cancer Chemother Pharmacol 2013; 71: 523-530.
[32] Li L, Fath MA, Scarbrough PM, Watson WH and Spitz DR. Combined inhibition of glycolysis, the pentose cycle, and thioredoxin metabolism selectively increases cytotoxicity and oxidative stress in human breast and prostate cancer. Redox Biol 2015; 4: 127-135.
[33] Liu W, Woolbright BL, Pirani K, Didde R, Abbott E, Kaushik G, Martin P, Hamilton-Reeves J, Taylor JA 3rd, Holzbeierlein JM, Anant S and Lee EK. Tumor M2-PK: a novel urine marker of bladder cancer. PLoS One 2019; 14: e0218737.
[34] Zhu Q, Hong B, Zhang L and Wang J. Pyruvate kinase M2 inhibits the progression of bladder cancer by targeting MAKP pathway. J Cancer Res Ther 2018; 14: S616-S621.
[35] Chai YJ, Yi JW, Oh SW, Kim YA, Yi KH, Kim JH and Lee KE. Upregulation of SLC2 (GLUT) family genes is related to poor survival outcomes in papillary thyroid carcinoma: analysis of data from The Cancer Genome Atlas. Surgery 2017; 161: 188-194.
[36] Kim E, Jung S, Park WS, Lee JH, Shin R, Heo SC, Choe EK, Lee JH, Kim K and Chai YJ. Upregulation of SLC2A3 gene and prognosis in colorectal carcinoma: analysis of TCGA data. BMC Cancer 2019; 19: 302.
[37] Jiang Y, Huo Z, Qi X, Zuo T and Wu Z. Copper-induced tumor cell death mechanisms and antitumor theragnostic applications of copper complexes. Nanomedicine (Lond) 2022; 17: 303-324.
[38] Prajapati N, Karan A, Khezerlou E and DeCoster MA. The immunomodulatory potential of copper and silver based self-assembled metal organic biohybrids nanomaterials in cancer theranostics. Front Chem 2020; 8: 629835.
[39] Tsvetkov P, Coy S, Petrova B, Dreishpoon M, Verma A, Abdusamad M, Rossen J, Joesch-Cohen L, Humeidi R, Spangler RD, Eaton JK, Frenkel E, Kocak M, Corsello SM, Lutsenko S, Kanarek N, Santagata S and Golub TR. Copper induces cell death by targeting lipoylated TCA cycle proteins. Science 2022; 375: 1254-1261.
[40] Zhang Z, Yu Y, Li P, Wang M, Jiao W, Liang Y and Niu H. Identification and validation of an immune signature associated with EMT and metabolic reprogramming for predicting prognosis and drug response in bladder cancer. Front Immunol 2022; 13: 954616.
[41] Zheng Z, Mao S, Zhang W, Liu J, Li C, Wang R and Yao X. Dysregulation of the immune microenvironment contributes to malignant progression and has prognostic value in bladder cancer. Front Oncol 2020; 10: 542492.
[42] Rana J and Biswas M. Regulatory T cell therapy: current and future design perspectives. Cell Immunol 2020; 356: 104193.
[43] Dees S, Ganesan R, Singh S and Grewal IS. Regulatory T cell targeting in cancer: emerging strategies in immunotherapy. Eur J Immunol 2021; 51: 280-291.
[44] Wang SS, Liu W, Ly D, Xu H, Qu L and Zhang L. Tumor-infiltrating B cells: their role and application in anti-tumor immunity in lung cancer. Cell Mol Immunol 2019; 16: 6-18.
[45] Wang L, Shi J, Liu S, Huang Y, Ding H, Zhao B, Liu Y, Wang W, Yang J and Chen Z. RAC3 inhibition induces autophagy to impair metastasis in bladder cancer cells via the PI3K/AKT/mTOR pathway. Front Oncol 2022; 12: 915240.